# A 7μW Offset-and Temperature-Compensated pH-to-Digital Converter

Heidary Shalmany, Saleh; Merz, Matthias; Fekri, Ali; Chang, Zu-yao; Hoofman, Romano J.O.M.; Pertijs, Michiel A.P.

**DOI**
10.1155/2017/6158689

**Publication date**
2017

**Document Version**
Final published version

**Published in**
Journal of Sensors (online)

Hindawi
Journal of Sensors
Volume 2017, Article ID 6158689, 8 pages
https://doi.org/10.1155/2017/6158689

*Research Article*

# A 7 $\mu$W Offset- and Temperature-Compensated pH-to-Digital Converter

**Saleh Heidary Shalmany,[1] Matthias Merz,[2] Ali Fekri,[3] Zu-yao Chang,[1] Romano J. O. M. Hoofman,[2] and Michiel A. P. Pertijs[1]**

[1]*Electronic Instrumentation Laboratory, Delft University of Technology, Mekelweg 4, 2628 CD Delft, Netherlands*
[2]*NXP Semiconductors, Interleuvenlaan 80, 3001 Leuven, Belgium*
[3]*AMS AG, Coveliersstraat 15, 2600 Antwerpen, Belgium*

Correspondence should be addressed to Michiel A. P. Pertijs; m.a.p.pertijs@tudelft.nl

Received 29 August 2016; Revised 20 November 2016; Accepted 7 December 2016; Published 29 January 2017

Academic Editor: Lucio Pancheri



This paper demonstrates a micropower offset- and temperature-compensated smart pH sensor, intended for use in battery-powered RFID systems that monitor the quality of perishable products. Low operation power is essential in such systems to enable autonomous logging of environmental parameters, such as the pH level, over extended periods of time using only a small, low-cost battery. The pH-sensing element in this work is an ion-sensitive extended-gate field-effect transistor (EGFET), which is incorporated in a low-power sensor front-end. The front-end outputs a pH-dependent voltage, which is then digitized by means of a co-integrated incremental delta-sigma ADC. To compensate for the offset and temperature cross-sensitivity of the EGFET, a compensation scheme using a calibration process and a temperature sensor has been devised. A prototype chip has been realized in a 0.16 $\mu$m CMOS process. It occupies $0.35 \times 3.9$ mm$^2$ of die area and draws only 4 $\mu$A from a 1.8 V supply. Two different types of custom packaging have been used for measurement purposes. The pH sensor achieves a linearity of better than ±0.1 for pH values ranging from 4 to 10. The calibration and compensation scheme reduces errors due to temperature cross-sensitivity to less than ±0.1 in the temperature range of 6°C to 25°C.

## 1. Introduction

Of the food produced globally for human consumption, about one third is lost or wasted [1]. In particular in industrialized countries, a substantial part of this waste concerns food that is, in principle, suitable for consumption, but that is discarded due to expiring "best-before" dates. This is mostly due to the fact that, at present, due-dates of perishables are mainly estimated from past historical knowledge of the product degradation, which, in most cases, underestimates the actual shelf life.

The quality of perishable goods can be determined more precisely if accurate information is available about the actual conditions that a particular product has been kept in. This could be done by means of a small and low-cost sensor tag that monitors relevant environmental parameters (such as temperature, humidity, pH level, $O_2$ concentration, and $CO_2$ concentration) [2]. Among these parameters, the pH level is particularly important for quality monitoring of meat- and fish-based products. The pH decay of meat postmortem (from ~7.5 to close to 5) can also be an indicator for the eating quality (i.e., tenderness) [3, 4].

Such a sensor tag could be equipped with radio-frequency identification (RFID) technology for communication and a thin-film battery to provide energy for data logging [2, 5]. To comply with the limited power and energy available in such a system, a power- and energy-efficient pH sensor is required. This work targets a power consumption of less than 10 $\mu$W and an energy consumption of less than 1 $\mu$J per pH measurement. Moreover, a pH sensor with co-integrated circuitry that provides a digital output is preferred for this application, since it is robust to external interference and its output can be readily processed, for example, by a microcontroller [6].

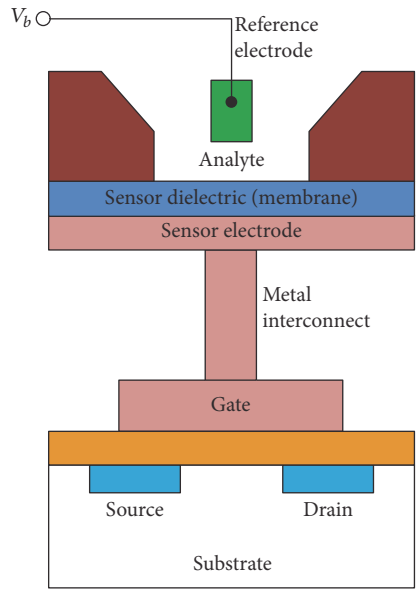


Figure 1: Diagram of the extended-gate field-effect transistor (EGFET).

An ion-sensitive field-effect transistor (ISFET) is a promising candidate for implementation of a portable and low-cost pH sensor, as it is compatible with CMOS technology [7–12]. By embedding an ISFET in a translinear loop composed of MOS transistors biased in the weak-inversion region, [7] demonstrates an ultra-low power (sub-microamp) current-mode pH sensor; however, it does not provide a digital output. In [8], a pH sensor with digital output (a "smart" pH sensor) is reported, but this design consumes 2.1 mW. In order to make the sensor more robust to common-mode errors, it uses an ISFET in a differential structure together with an ion-insensitive FET (or so-called reference FET, REFET). An 80 $\mu$W pH sensor system, reported in [9], took a major step towards a micropower smart pH-sensor. It combines an array of ISFETs interfaced with a co-integrated analog-to-digital converter (ADC).

ISFET-based pH sensors are strongly cross-sensitive to ambient temperature: their pH sensitivity is proportional to absolute temperature (PTAT) [4, 11, 13–17]. This should be properly addressed in applications where the temperature is expected to vary, as is the case in the logistic chain of perishable products. By means of an algorithmic temperature-compensation approach and a dynamic biasing current technique, [14, 16] address this issue in a pH range of 4 to 9 and temperature range of 22°C to 50°C and of 23°C to 40°C, respectively. In [11], an ISFET-based pH sensor is combined with a p-n junction diode for combined monitoring of pH and temperature, but without explicitly addressing compensation for temperature cross-sensitivity. In [17], the cross-sensitivity to temperature is addressed by using a co-integrated temperature-sensing system that is based on the temperature-dependent characteristics of a MOSFET's threshold voltage. After performing temperature compensation, the ISFET's temperature sensitivity is reduced by a factor of 10. These works, however, do not provide a digital output.

In this work we present a *micropower smart pH sensor*, for battery-powered pH-monitoring applications. We have reported preliminary results of this sensor in [6]. This paper describes the sensor in more detail and introduces a digital temperature-compensation scheme together with additional measurement results obtained with a new packaging approach. The sensor employs an extended-gate field-effect transistor (EGFET) for pH sensing and substrate bipolar transistors for temperature sensing. A shared ADC digitizes both pH and temperature information in a time-multiplexed manner, while consuming only 7 $\mu$W.

This paper is organized as follows. Section 2 introduces the basic operating principle of an EGFET and two important nonidealities: temperature cross-sensitivity and offset voltage. In Section 3, the proposed method for temperature and offset compensation is presented. The low-power sensor front-end and the delta-sigma ($\Delta\Sigma$) analog-to-digital converter (ADC) are described in Sections 4 and 5, respectively. The paper continues with a discussion on the implementation, packaging, and measurement results in Section 6. Section 7 concludes the paper.

## 2. Extended-Gate Field-Effect Transistor (EGFET)

A schematic diagram of the sensing element, which includes an EGFET and a reference electrode, is shown in Figure 1 [6]. The EGFET is basically a MOSFET (metal-oxide field-effect transistor) of which the gate is extended to the passivation layer of the die via metal interconnect. On this layer, the sensor dielectric (sensor membrane) is deposited to be in direct contact with the target analyte. The dielectric is made of $Ta_2O_5$ deposited by a highly conformal chemical vapor deposition (CVD) process, so as to obtain a tight layer stack and thus prevent leakage and drift. The reference electrode used in this work is a commercial glass electrode. In future work, this will be replaced by a reference electrode integrated in the package of the sensor (see Section 6.1). A bias voltage $V_b$, applied to this electrode, experiences a pH-dependent voltage shift $\Delta V_{\mathrm{pH}}$ at the dielectric-analyte interface, modulating the threshold voltage $V_{\mathrm{th}}$ of the MOSFET.

The threshold-voltage shift $\Delta V_{\mathrm{pH}}$ has a sensitivity that is proportional to absolute temperature (PTAT) and roughly equals 55 mV/pH at room temperature [11, 13–17]. Moreover, due to trapped charge between the MOSFET gate and the sensor dielectric, $\Delta V_{\mathrm{pH}}$ shows an offset voltage $V_{\mathrm{os}}$ (max. ±300 mV in our process), which we assume to be nominally temperature independent. The shift in EGFET threshold voltage can therefore be expressed as

$$\Delta V_{\mathrm{pH}} = A \cdot T \cdot \left(\mathrm{pH} - \mathrm{pH}_0\right) + V_{\mathrm{os}} \tag{1}$$

in which $T$ [K] is the absolute temperature, pH is the pH level of the analyte, and $A$ and $\mathrm{pH}_0$ are constants defining the sensitivity and zero point of the pH-dependent voltage shift. Any die-to-die variations in these constants are corrected for during system calibration. The next section discusses the

method used to mitigate the effects of temperature variation and $V_{os}$ on the pH reading.

## 3. Temperature and Offset-Voltage Compensation

By means of a calibration process and temperature information obtained from an embedded temperature sensor, the effects of offset voltage and temperature variation are compensated. To characterize the EGFET's response to an analyte, the parameters in (1) should be first calibrated. During the calibration process, the sensor is exposed to a buffer solution with a known pH level (measured by a reference pH meter). The temperature is measured by the sensor and therefore does not have to be accurately stabilized. The on-chip ADC then digitizes the resulting $\Delta V_{pH}$ with respect to a constant reference voltage $V_{ext}$, which is currently implemented off chip, but can be readily integrated using a band-gap reference circuit. This gives a digital representation of $\Delta V_{pH}$ as

$$\mu_1 = \frac{\Delta V_{pH}}{V_{ext}}. \tag{2}$$

To obtain the temperature information, the ADC also digitizes $\Delta V_{pH}$ with respect to an on-chip generated PTAT voltage $V_{PTAT}$, resulting in digital value

$$\mu_2 = \frac{\Delta V_{pH}}{V_{PTAT}}, \tag{3}$$

and then, by digitally dividing the results of these two conversions, temperature is calculated:

$$\frac{\mu_1}{\mu_2} = \frac{V_{PTAT}}{V_{ext}} = b \cdot T \tag{4}$$

in which $b$ is a constant, obtained from a temperature calibration process. Thus, three parameters in (1), $\Delta V_{pH}$, pH, and $T$, can be obtained.

In order to calculate the other three parameters, namely, $A$, $pH_0$, and $V_{os}$, the above process should be performed for another two times: once with the same buffer solution but at a different temperature and once with a different buffer solution (different pH level) and at an arbitrary temperature. By solving the resulting set of three equations obtained from this calibration process, the three unknown calibration parameters $A$, $pH_0$, and $V_{os}$ can then be calculated.

During the normal operation of the sensor, $\Delta V_{pH}$ and $T$ are digitized in the same way by means of the two aforementioned analog-to-digital conversions. The pH level of the target analyte is then calculated by using the three calibration parameters as

$$pH = \frac{\left(\Delta V_{pH} - V_{os}\right)}{(A \cdot T)} + pH_0. \tag{5}$$

## 4. Front-End Circuits

The front-end circuits for pH and temperature measurement are described in this section.

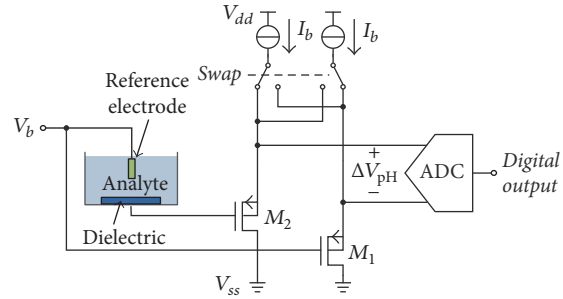


Figure 2: Differential source-follower with embedded EGFET followed by a 1st-order incremental ΔΣ ADC.

*4.1. pH Sensor.* Figure 2 shows the pH-sensor front-end which employs one EGFET ($M_2$) and one regular MOSFET ($M_1$) as the input-pair of a differential source-follower (SF). Both the EGFET and the regular MOSFET have an aspect ratio $W/L$ of 8 $\mu$m/2 $\mu$m, and each is biased at a current level $I_b$ of only 80 nA. A bias voltage $V_b$ is applied to both the gate terminal of the MOSFET and the reference electrode of the EGFET. The voltage at the source terminal of the MOSFET is then $V_{S,MOS} = V_b + V_{SG,MOS}$, where $V_{SG,MOS}$ is the source-gate voltage of the MOSFET, while the voltage at the source terminal of the EGFET equals $V_{S,EGFET} = V_b + V_{SG,EGFET}$.

Since the input-pair devices are equally sized and biased at the same current level, the source-gate voltages of the two MOSFETs are nominally equal, leading to a differential ADC input voltage equal to the pH-dependent threshold shift $\Delta V_{pH}$ of the EGFET. Any (pH-independent) threshold-voltage mismatch between the MOSFETs can be accounted for in $\Delta V_{pH}$ by appropriate values for $V_{os}$ and $pH_0$ in (1) and will thus be compensated by the calibration process. It should also be mentioned that connecting the source and the body terminals of each input device together eliminates errors due to the transistors' body effect.

The bias voltage $V_b$ should be chosen to provide enough voltage swing capability at the SF output; however, it does not need to be accurately controlled, as any error in $V_b$ will translate to a common-mode signal for the differential SF circuit, which to first order will not influence the differential output voltage. The two current sources are periodically switched between the MOSFET and the EGFET (chopping technique) in order to average out the error caused by mismatch in their current levels [18].

*4.2. Temperature Sensor.* By exploiting the temperature-dependent base-emitter voltage $V_{BE}$ of the parasitic substrate bipolar transistors (PNPs) available in standard CMOS technology, the temperature information is extracted. The base-emitter voltage of a bipolar transistor biased in its forward-active region is described by the following well-known equation [18, 19]:

$$V_{BE} = \frac{kT}{q} \ln\left(\frac{I_C}{I_S}\right) \tag{6}$$

in which $k$ is Boltzmann's constant, $q$ is the electron charge, $T$ is the absolute temperature, $I_C$ is the collector current, and $I_S$

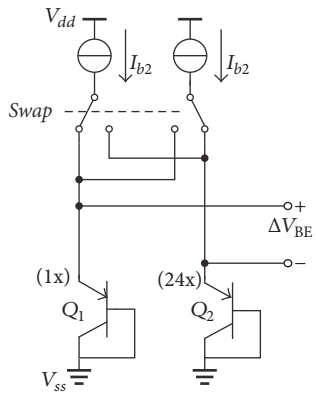


Figure 3: Substrate PNPs generating PTAT voltage.

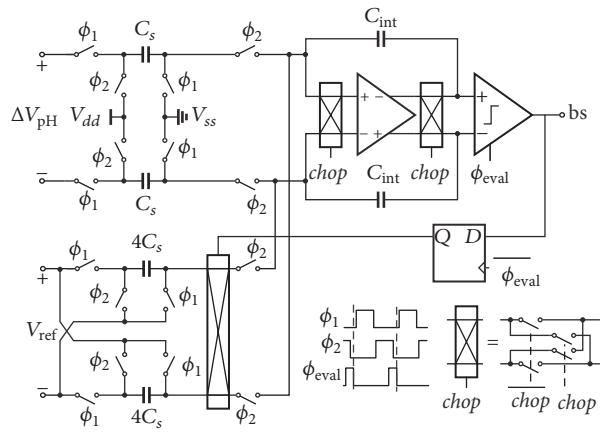


Figure 4: Circuit diagram of the fully differential first-order ΔΣ modulator with the associated timing diagram.

is the transistor's saturation current, which is proportional to the transistor's emitter area. While temperature dependent, $V_{BE}$ is not a very reproducible function of temperature due to the large tolerance of the saturation current $I_S$ in CMOS technology. The resulting spread in $V_{BE}$ can lead to temperature errors as large as ±3°C [18]. However, the difference between the base-emitter voltages, $\Delta V_{BE}$, of two PNPs that are biased at different current densities is much more accurate, since it is insensitive to $I_S$.

Figure 3 shows two parasitic substrate PNPs, $Q_1$ and $Q_2$, with an emitter-area ratio of $p = 24$, each biased at only 100 nA emitter current. The difference between the base-emitter voltages of these two PNPs, $\Delta V_{BE}$, has a well-defined PTAT characteristic [18, 19]

$$\Delta V_{BE} = V_{BE1} - V_{BE2} = \frac{kT}{q} \ln(p) \tag{7}$$

which, at room temperature, is about 85 mV.

The reason for choosing $p = 24$ is that it biases both $Q_1$ and $Q_2$ in the constant-beta region at the 100 nA current level, so that the collector-current-density ratio is not affected by the finite current-gain of the transistors [18]. Furthermore, to reduce the effect of device mismatch on the emitter-area ratio, it allows a common-centroid layout of $Q_1$ and $Q_2$, in which $Q_1$ is the middle device of an array of 5 × 5 equally sized PNPs and $Q_2$ is composed of the remaining 24 devices. To mitigate the effects of mismatch of the current sources, they are periodically interchanged during a measurement using a chopper switch, so that errors due to their mismatch average out.

## 5. Delta-Sigma (ΔΣ) ADC

Given the slowly varying nature of the pH and the temperature signals, which have a bandwidth in the order of a few tens of Hertz, an incremental ΔΣ ADC is chosen, which exploits oversampling to digitize its input signal [18, 20]. Figure 4 shows the circuit diagram of the fully differential first-order ΔΣ ADC. It consists of a switched-capacitor integrator, built around an operational transconductance amplifier (OTA), and a clocked comparator. The input of this ADC is the voltage $\Delta V_{pH}$ produced by the pH-sensor front-end circuit. To implement the compensation method discussed in Section 3, the (differential) reference voltage $V_{ref}$ of the ADC is provided either by the PTAT voltage $\Delta V_{BE}$ generated by the temperature sensor front-end circuit or by an external reference voltage $V_{ext}$.

The ADC works as follows. During $\varphi_1$, the input capacitors $C_S$ of 50 fF sample the input voltage $\Delta V_{pH}$, while the feedback capacitors $4C_S$ sample the voltage $2V_{ref}$ (either $V_{ext}$ or $\Delta V_{BE}$). During $\varphi_2$, capacitors $C_S$ transfer a charge $C_S \cdot \Delta V_{pH}$ to the integration capacitors $C_{int}$, which equal 250 fF. At the same time, the capacitors $4C_S$ transfer a charge of $\pm 4C_s \cdot 3V_{ref}$ to the integration capacitors, with a polarity that depends on the bitstream output bs of the comparator (0 or 1). The latter is determined by the polarity of the integrator's output voltage at the rising edge of the $\phi_{eval}$ signal. This establishes a negative feedback that drives the integrator's output voltage to zero. As a result, after $N$ clock cycles, the charge contributed by $\Delta V_{pH}$ will be balanced by the charge contributed by $V_{ref}$.

$$N \cdot C_S \cdot \Delta V_{pH} - M \cdot 12 \cdot C_S \cdot V_{ref} + (N - M) \cdot 12 \cdot C_S \cdot V_{ref} \approx 0, \tag{8}$$

where $M$ is the number of clock cycles during which bs = 1. Hence, the average of ADC's output bitstream is

$$\mu_1 = \frac{M}{N} = \frac{\Delta V_{pH}}{(24V_{ref})} + \frac{1}{2} \tag{9}$$

from which the ratios $\mu_1$ and $\mu_2$ given by (2) and (3), required for the pH sensing and temperature compensation, can easily be obtained by using first $\Delta V_{BE}$ and then $V_{ext}$ for $V_{ref}$. Given that $0 \le \mu \le 1$, the ADC can digitize values of $\Delta V_{pH}$ in the range of $\pm 12 \cdot V_{ref}$, which is chosen to accommodate the total variation of $\Delta V_{pH}$, which can be as large as ±500 mV over the pH range of 4 to 10 (including the maximum $V_{os}$ of ±300 mV).

The OTA used in the integrator has a folded-cascode topology. Errors due to its offset and $1/f$ noise are mitigated by means of chopping. The clocked comparator consists of a dynamic latch preceded by two preamplifier stages with an approximate gain of 5x each. The ADC runs at a clock

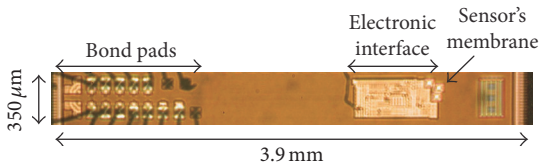


Figure 5: Chip micrograph.

frequency of 25 kHz and draws a supply current of 3.5 $\mu$A, of which 300 nA is consumed by the OTA and 3.2 $\mu$A by the comparator. The majority of the supply current is consumed by an unintended shoot-through current in a logic gate at the output of the comparator. This can easily be mitigated in a redesign, after which the supply current should be reduced to approximately 150 nA.

## 6. Experimental Results

*6.1. Implementation and Packaging.* The pH-to-digital converter was realized in a standard 0.16 $\mu$m CMOS process. Figure 5 shows a micrograph of the chip, which measures 0.35 mm × 3.9 mm. The bond pads and sensor's membrane with associated interface circuit are placed at two opposite sides of the die. This will facilitate a type of system packaging in which the bond-wires are isolated from the analyte when it is in contact with the sensor's dielectric. The dies were isolated using the standard passivation stack of the employed CMOS process. The passivation layer was locally opened on top of the sensor electrodes, allowing $Ta_2O_5$ to be deposited by CVD, yielding a device that was stable at least for several days. The sensor's dielectric, laid out on the passivation layer besides the electronic interface, measures 30 $\mu$m × 30 $\mu$m.

Two different types of packaging have been used for characterization purposes:

(1) For initial characterization, dies have been packaged in 40-pin ceramic dual in-line (DIL) packages with a small plastic cubic container (measuring 0.5 $cm^3$) glued on top of the die to hold the analyte, as shown in Figure 6(a). To facilitate water-tight gluing of this container, a piece of silicon larger than the chip was diced out of the wafer.

(2) For further characterization, a packaging concept was created that considers the requirements for use in a "wet" environment. As shown in Figure 6(b), the package is shaped in such a way that it can be easily immersed into test buffer solution while moulding compound protects all metallic tracks. For this packaging approach, dies were glued and wire bonded to a custom-designed printed-circuit board (PCB), after which the PCB and the die were encapsulated using an open-cavity moulding process. For access of liquids to the sensor area, open windows have been designed in the package. A second window is also available for integration of a reference electrode into the stick, although the experiments reported in this paper still rely on an external glass reference electrode. Experiments showed that this encapsulation is certainly robust enough for several days in liquid contact.

As shown in Figure 6(c), the moulded stick is connected to a small custom printed-circuit board (PCB), which contains an ARM microcontroller, a battery, and several other auxiliary components, including a connector for serial communication. It can autonomously log pH and temperature readings and communicate the results via a wired serial connection (RS-232 interface) to a PC or laptop.

*6.2. Measurements.* To evaluate the pH measurement performance with the first package, the plastic container was filled with buffer solutions with pH values ranging from 3 to 10 in steps of approximately 1, all at room temperature. The pH of these buffer solutions was measured using a calibrated pH meter. The experiment was performed in a dark room to minimize the effect of the sensor's cross-sensitivity to light. Since in this experiment the temperature was kept constant, a two-point calibration was performed at pH levels 4 and 7. Using an external reference electrode, the chip reliably digitizes the pH level (Figure 7). Relative to a least-squares linear fit, the nonlinearity is equivalent to less than ±0.1 pH. Note that for every pH step shown in this figure the data of 10 minutes of cleaning and refilling the plastic cubic container have been removed.

The system's digital output has a sensitivity of around 5%/pH relative to the full output scale which corresponds to pH-sensitivity of $\Delta V_{pH}$ roughly equal to 55 mV/pH, which is in good agreement with the theoretically expected value. The sensor's resolution was determined by calculating the standard deviation of repeated measurements at a constant pH level and temperature. In a conversion time of 20 ms, the sensor provides a resolution of 0.05 pH.

The sensor draws a supply current of only 4 $\mu$A from a 1.8 V supply, dominated by the supply current of the ADC, which, as mentioned, can be further reduced. This corresponds to a power consumption of 7 $\mu$W and an energy per measurement of 140 nJ. The sensor will typically not be operated continuously in a monitoring application. In [4], for instance, a 5-minute measurement interval is used. The average power consumed by the sensor, even with some overhead included for data processing, is then readily negligible compared to the standby power consumed by a low-power microcontroller in a datalogger, which is typically at the $\mu$W level [5]. This means that the charge of a small printed or flexible battery (on the order of 10 mAh) will suffice for >100 days of operation [5]. Note that in practice the useful operation time will then be limited by the long-term stability of the sensor.

To evaluate the temperature-sensing performance, one prototype chip has been placed in a climate chamber along with a calibrated Pt100 thermometer. Figure 8 shows the temperature measured using the chip over the range of −5 to 45°C in steps of 5°C, along with the error of a linear fit of the measured data. The result shows that, after a two-point calibration, an error below ±0.1°C can be obtained, making the approach suitable for temperature cross-sensitivity

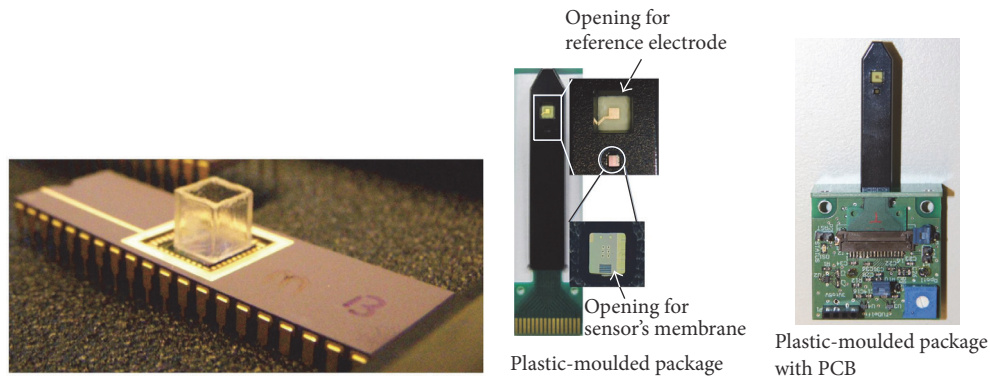


FIGURE 6: 40-pin ceramic DIL package with a small plastic cubic container (a) and plastic-moulded package (b), with custom-designed PCB for data logging (c).

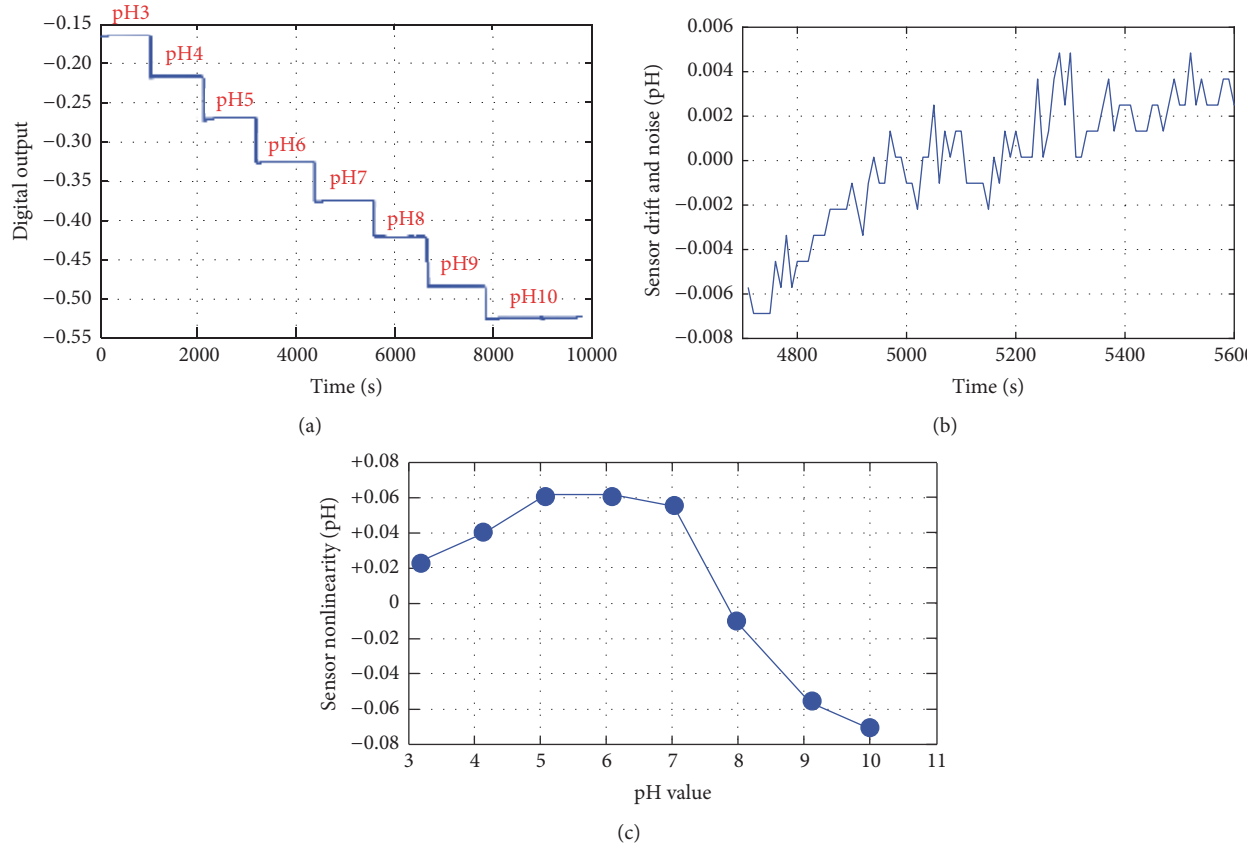


FIGURE 7: Measured digital output of the sensor, as expressed in (2), for buffer solutions of different pH levels (a), pH-sensor output drift and noise at pH7 (b), and sensor nonlinearity versus pH of buffer solution (c). (Note that for every pH step, the data of 10 minutes of cleaning and refilling the plastic cubic container have been removed.)

cancellation. In principle, it should be possible to achieve similar performance after a one-point calibration if further dynamic error-correction techniques are applied in the front-end circuit, for instance, to address errors due to the inaccuracy of the emitter-area ratio of the bipolar transistors [18]. In this design, however, a two-temperature calibration is also needed for the pH measurement and so does not come at significant additional cost.

To evaluate the temperature cross-sensitivity compensation approach and the spread between different sensors, three plastic-moulded packaged sensors were exposed to three different commercial buffer solutions with pH levels

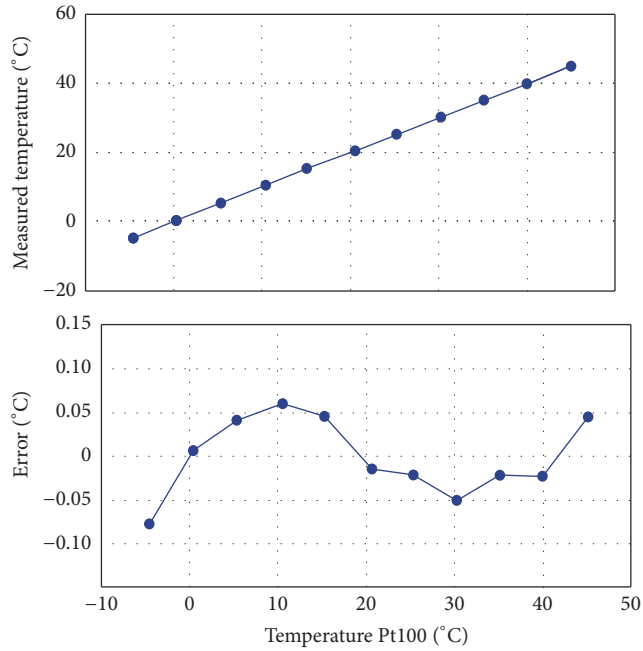


Figure 8: Temperature measured using the smart pH-sensor chip, along with the measured error with respect to a Pt100 thermometer.

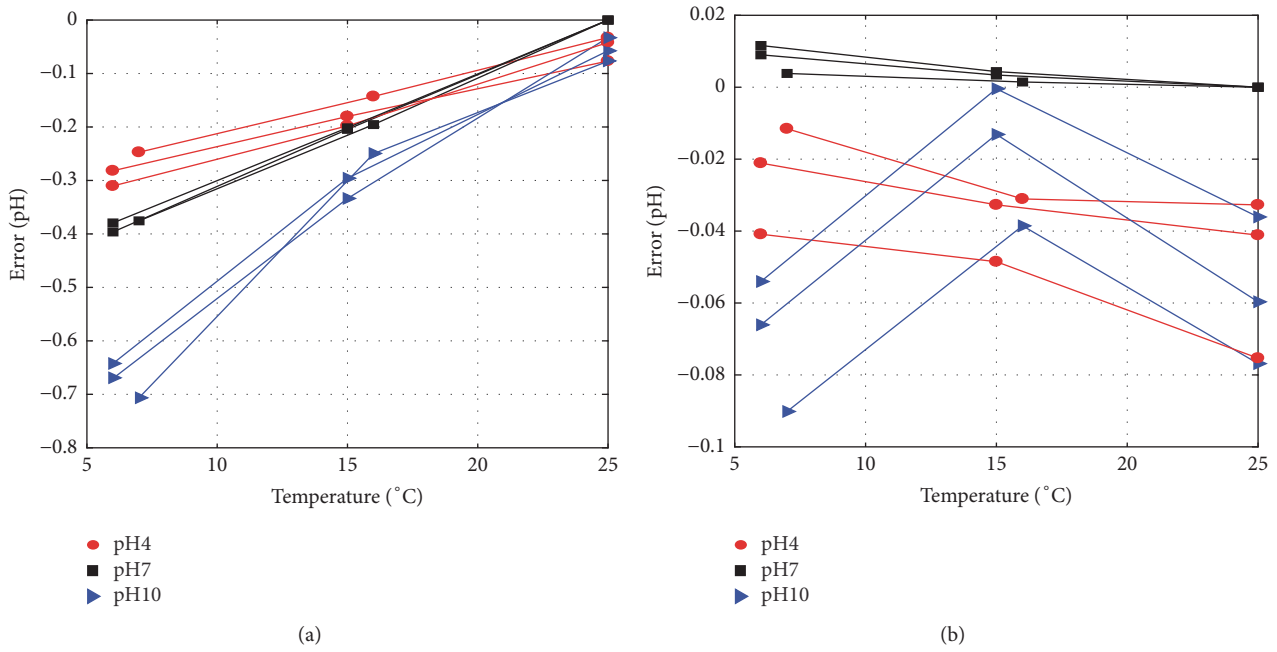


Figure 9: Error in the digital pH reading of three sensors after offset compensation and before (a) and after (b) temperature compensation.

of 4, 7, and 10, each at three temperature points roughly equal to 6°C, 16°C, and 25°C. Each sensor was individually calibrated/characterized at three points: pH 4 at 25°C, pH 7 at 25°C, and pH 7 at 16°C. As shown in Figure 9, after offset compensation and before temperature compensation, the three sensors show pH errors up to 0.8 pH. After temperature compensation using the approach described in Section 3, the errors are significantly reduced. As to be expected, the error is smallest for pH level 7, for which the temperature dependency was calibrated. But also at the other pH levels, the error is reduced to less than ±0.1 pH, confirming the validity of the model for the sensor's temperature cross-sensitivity given by (1) and the effectiveness of the proposed compensation approach.

## 7. Conclusion

The design, implementation, and experimental characterization of an EGFET-based smart pH sensor have been reported in this paper. The EGFET is embedded in a low-power differential source-follower circuit, followed by a first-order incremental $\Delta\Sigma$ ADC. In order to cancel the sensor's temperature cross-sensitivity, a temperature-sensing mechanism has been devised by digitizing an on-chip PTAT voltage with respect to a constant external voltage. Two different types of packaging have been used in this work. The first is a 40-pin ceramic DIL package with a small plastic cubic container, with which at room temperature a nonlinearity below ±0.1 in a pH range from 4 to 10 is achieved. The second is a plastic-moulded package, for which three sensors have been tested at three pH levels of 4, 7, and 10 and at three temperature points of 6°C, 16°C, and 25°C. After a three-point calibration and temperature compensation, errors due to temperature cross-sensitivity are reduced to less than ±0.1 pH. The sensor has a resolution of 0.05 pH in a 20 ms measurement time. It consumes only 4 $\mu$A from a 1.8 V supply, corresponding to a power consumption of only 7 $\mu$W and an energy consumption of less than 140 nJ per pH measurement. This level of power and energy consumption demonstrates the feasibility of this sensor for use in RFID sensor tags.

## Competing Interests

The authors declare that there is no conflict of interests regarding the publication of this paper.

## Acknowledgments

This research was performed in context of the Catrene PASTEUR project. The authors would like to acknowledge all partners who contributed to this work and in particular Boschman Technologies for providing the moulded plastic package.

## References

[1] V. Prakash, J. Ambuko, W. Belik et al., "Food losses and waste in the context of sustainable food systems," A Report by the High Level Panel of Experts on Food Security and Nutrition of the Committee on World Food Security, Food and Agriculture Organization of the United Nations, Rome, Italy, 2014, http://www.fao.org/cfs/cfs-hlpe.

[2] M. Vanderroost, P. Ragaert, F. Devlieghere, and B. De Meulenaer, "Intelligent food packaging: the next generation," *Trends in Food Science & Technology*, vol. 39, no. 1, pp. 47–62, 2014.

[3] L. P. Yu and Y. B. Lee, "Effects of postmortem pH and temperature on bovine muscle structure and meat tenderness," *Journal of Food Science*, vol. 51, no. 3, pp. 774–780, 1986.

[4] J. Frisby, D. Raftery, J. P. Kerry, and D. Diamond, "Development of an autonomous, wireless pH and temperature sensing system for monitoring pig meat quality," *Meat Science*, vol. 70, no. 2, pp. 329–336, 2005.

[5] T. Unander, J. Sidén, and H.-E. Nilsson, "Designing of RFID-based sensor solution for packaging surveillance applications," *IEEE Sensors Journal*, vol. 11, no. 11, pp. 3009–3018, 2011.

[6] S. H. Shalmany, M. Merz, A. Fekri, Z. Chang, R. Hoofman, and M. A. P. Pertijs, "A 7$\mu$W pH-to-digital converter for quality monitoring of perishable products," in *Proceedings of the 17th International Conference on Solid-State Sensors, Actuators and Microsystems (TRANSDUCERS and EUROSENSORS '13)*, pp. 1747–1750, Barcelona, Spain, June 2013.

[7] L. M. Shepherd and C. Toumazou, "A biochemical translinear principle with weak inversion ISFETs," *IEEE Transactions on Circuits and Systems I: Regular Papers*, vol. 52, no. 12, pp. 2614–2619, 2005.

[8] P. A. Hammond, D. Ali, and D. R. S. Gumming, "Design of a single-chip pH sensor using a conventional 0.6-$\mu$m CMOS process," *IEEE Sensors Journal*, vol. 4, no. 6, pp. 706–712, 2004.

[9] W. P. Chan, B. Premanode, and C. Toumazou, "An integrated ISFETs instrumentation system in standard CMOS technology," *IEEE Journal of Solid-State Circuits*, vol. 45, no. 9, pp. 1923–1934, 2010.

[10] K. Nakazato, "An integrated ISFET sensor array," *MDPI Sensors*, vol. 9, no. 11, pp. 8831–8851, 2009.

[11] M. Futagawa, T. Iwasaki, H. Murata, M. Ishida, and K. Sawada, "A miniature integrated multimodal sensor for measuring pH, EC and temperature for precision agriculture," *MDPI Sensors*, vol. 12, no. 6, pp. 8338–8354, 2012.

[12] C. Jimenez-Jorquera, J. Orozco, and A. Baldi, "ISFET based microsensors for environmental monitoring," *Sensors*, vol. 10, no. 1, pp. 61–83, 2010.

[13] Y.-L. Chin, J.-C. Chou, Z.-C. Lei, T.-P. Sun, W.-Y. Chung, and S.-K. Hsiung, "Titanium nitride membrane application to extended gate field effect transistor pH sensor using VLSI technology," *Japanese Journal of Applied Physics*, vol. 40, no. 11, pp. 6311–6315, 2001.

[14] P. K. Chan and D. Y. Chen, "A CMOS ISFET interface circuit with dynamic current temperature compensation technique," *IEEE Transactions on Circuits and Systems I: Regular Papers*, vol. 54, no. 1, pp. 119–129, 2007.

[15] Y.-L. Chin, J.-C. Chou, T.-P. Sun, W.-Y. Chung, and S.-K. Hsiung, "A novel pH sensitive ISFET with on chip temperature sensing using CMOS standard process," *Sensors and Actuators, B: Chemical*, vol. 76, no. 1-3, pp. 582–593, 2001.

[16] D. Y. Chen and P. K. Chan, "An intelligent ISFET sensory system with temperature and drift compensation for long-term monitoring," *IEEE Sensors Journal*, vol. 8, no. 12, pp. 1948–1959, 2008.

[17] W.-Y. Chung, Y.-T. Lin, D. G. Pijanowska et al., "New ISFET interface circuit design with temperature compensation," *Microelectronics Journal*, vol. 37, no. 10, pp. 1105–1114, 2006.

[18] M. A. P. Pertijs and J. H. Huijsing, *Precision Temperature Sensors in CMOS Technology*, Springer, Dordrecht, The Netherlands, 2006.

[19] G. C. M. Meijer, "Thermal sensors based on transistors," *Sensors and Actuators*, vol. 10, no. 1-2, pp. 103–125, 1986.

[20] J. Markus, J. Silva, and G. C. Temes, "Theory and applications of incremental $\Delta\Sigma$ converters," *IEEE Transactions on Circuits and Systems I: Regular Papers*, vol. 51, no. 4, pp. 678–690, 2004.